Smart Structures and Systems, *Vol. 30, No. 4 (2022) 339-351*
https://doi.org/10.12989/sss.2022.30.4.339

Structural system identification by measurement error-minimization observability method using multiple static loading cases

Jun Lei [1,2,3], Jose Antonio Lozano-Galant [4], Dong Xu [5], Feng-Liang Zhang*[3] and Jose Turmo [6]

[1] *Key Laboratory of Earthquake Engineering and Engineering Vibration, Institute of Engineering Mechanics, China Earthquake Administration, Harbin 150086, China*
[2] *Key Laboratory of Earthquake Disaster Mitigation, Ministry of Emergency Management, China*
[3] *School of Civil and Environmental Engineering, Harbin Institute of Technology, Shenzhen, China*
[4] *Department of Civil Engineering, University of Castilla-La Mancha, Ciudad, Real, Spain*
[5] *Department of Bridge Engineering, Tongji University, Shanghai, China*
[6] *Department of Civil and Environmental Engineering, Universitat Politècnica de Catalunya, Barcelona, Spain*

(*Received June 20, 2021, Revised April 19, 2022, Accepted May 26, 2022*)

Abstract. Evaluating the current condition of existing structures is of primary importance for economic and safety reasons. This can be addressed by Structural System Identification (SSI). A reliable static SSI depends on well-designed sensor configuration and loading cases, as well as efficient parameter estimation algorithms. Static SSI by the Measurement Error-Minimizing Observability Method (MEMOM) is a model-based deterministic static SSI method that could estimate structural parameters from static responses. In the current state of the art, this method is only applicable when structures are subjected to one loading case. This might lead to lack of information in some local regions of the structure (such as the null curvatures zones). To address this issue, the SSI by MEMOM using multiple loading cases is proposed in this work. Observability equations obtained from different loading cases are concatenated simultaneously and an optimization procedure is introduced to obtain the estimations by minimizing the discrepancy between the predicted response and the measured one. In addition, a Genetic-Algorithm (GA)-based Optimal Sensor Placement (OSP) method is proposed to tackle the OSP problem under multiple static loading cases for the very first time. In this approach, the Fisher Information Matrix (FIM)'s determinant is used as the metric of the goodness of sensor configurations. The numerical examples of a 3-span continuous bridge and a 13-story frame, are analyzed to validate the applicability of the extended SSI by MEMOM and the GA-based OSP method.

Keywords: genetic algorithm; measurement errors; multiple loading cases; observability method; static response; optimization; stiffness matrix method; structural system identification

1. Introduction

During the construction and operation stages, infrastructure and civil structures suffer from irreversible deterioration due to various factors such as overloading, concrete cracking, concrete carbonation and reinforcement corrosion (Zhang *et al*. 2020). Consequently, these structures might fail to meet the public requirements regarding the normal use and safe operation. To avoid such undesirable situation, it is of primary importance to obtain their current condition to support the decision-making basis for the follow-up treatment. During the past decades, Structural System Identification (SSI) has emerged as a powerful tool to serve this purpose. The basic principle of SSI is that the change of the structural condition is reflected by the change of the structural parameters; and this can be revealed by the change in the structural response.

Regarding the types of external excitation, SSI can be categorized as dynamic (Brownjohn *et al*. 2008, Papadopoulos and Garcia 1998, Wang *et al*. 2001) and static (Abdo 2012, Bakhtiari-Nejad *et al*. 2005, Banan *et al*. 1994a, b, Ma and Solís 2018, Sanayei and Scampoli 1991, Sheena *et al*. 1982). As shown by their long history in civil engineering, static load tests provide important information on displacements, rotations and strains, serving as an appropriate alternative and an amendment to visual inspections and dynamic methods as deflections or strains are relatively easy to obtain (Nguyen *et al*. 2016). However, the majority of SSI research focuses on dynamic SSI. In dynamic SSI, it is common to assume no damping in the system and that the damage of the structure does not lead to the loss of mass (Papadopoulos and Garcia 1998, Wang *et al*. 2001). Effects of moisture and temperature conditions on the water content of concrete structures and, hence, on its mass, are usually neglected. These assumptions might introduce modelling errors in the parameter estimation (Lei *et al*. 2019). In addition, modal shapes are sensitive to structural damage but are hard to obtain accurately, especially in stiff structures. On the contrary, the acquisition of accurate frequency is less challenging but frequency is not very sensitive to structural damage (Farrar *et al*. 1994, Kim *et al*. 2003). Static response might be more sensitive to local damage while dynamic response provides a more

*Corresponding author, Ph.D., Professor,
E-mail: zhangfengliang@hit.edu.cn

Copyright © 2022 Techno-Press, Ltd.

ISSN: 1738-1584 (Print), 1738-1991 (Online)

accurate overall and distributed information about the structure (Brownjohn *et al*. 2008). In the static SSI, the basic equations are established on the equilibrium of nodal forces. Neither damping nor mass is involved (Wang *et al*. 2001), which allows static SSI to focus on identifying less unknown structural parameters. Also, current measurement devices for static tests are cheaper and more accurate than those for dynamic testing (Kourehli 2017).

Static SSI has been widely investigated for the purpose of condition assessment. Sheena *et al*. (1982) presented a method for improving the analytical stiffness matrix. After measuring a set of Degrees of Freedom (DOFs), spline functions were used to predict the remaining unmeasured DOFs. Then, the difference between the theoretical stiffness matrix and the real one was minimized by adjusting the element properties. Hajela and Soeiro (1990) classified the SSI into three types: equation error approach, output error approach and minimum deviation approach. Both static and eigenmodes of the structure were combined in the damage detection. Banan *et al*. (1994a, b) used an iterative optimization method to estimate the element properties based on two indices of discrepancy including the force and the displacement error estimation. Hjelmstad and Shin (1997) assumed that the baseline values of structural parameters were known and proposed adaptive parameter grouping algorithm to detect and evaluate structural damage. Abdo (2012) studied the relation between the change in static displacement curvature and the damage characteristics (location and severity). This method successfully detected and located damages in beam-like structures. However, in this method, a comparison with the structural response of the intact structure was required.

Static SSI is essentially the application of parameter estimation in structural systems. In parameter estimation, the classical observability problem is involved with the observability (existence and uniqueness) of the estimated parameters. The Observability Method (OM) has been applied in static SSI to determine the observability of the structural parameters by checking the null space of the coefficient matrix of observability equations (Lozano-Galant *et al*. 2013). These equations are obtained by reconstructing the static equilibrium equations via a series of algebraic operations. Nogal *et al*. (2015) proposed the Numerical Observability Method (NOM) that incorporated a numerical evaluation procedure in the original SSI by OM. The effect of measurement errors and simulation errors on the accuracy of the estimated parameters using SSI by NOM with minimum measurement sets were investigated. Lozano-Galant *et al*. (2015) proposed the observability tree method according to the mechanical connection between structural parameters and measurements. With this method, the measurement set with the minimum number of necessary measurements to ensure observability of all parameters is determined, which is referred as minimum measurement set. Lei *et al*. (2018) revealed the lacking nonlinear constraints in the observability equations in SSI by NOM and reintroduced these constraints by an optimization procedure. This method has also been applied in the SSI of structures where shear deformation cannot be neglected (Emadi *et al*. 2019, Tomàs *et al*. 2018) and in dynamic SSI using modal analysis (Peng *et al*. 2020). In order to improve the estimation by using redundant measurements, the SSI by Measurement Error Minimizing Observability Method (MEMOM) was proposed by Lei *et al*. (2019).

The quality of static SSI results depends on the following factors: (1) loading cases that activate the mechanical behavior of the structures to be identified; (2) the number and the spatial location of sensors that ensure the quality of the measurement raw data; and (3) efficient parameter estimation algorithms that exploit the essential information of structures from the loading cases and the measured response. In static SSI, the damage of structures might be concealed due to the limitation of the load paths (Chen *et al*. 2005), especially when only one loading case is used. This agrees with the observation that accurate estimation of bending structural parameters in null curvature zones is intractable (Emadi *et al*. 2019). These zones include those adjacent to the supports or near the inflection points of the bending moment diagram. Unfortunately, it is inevitable to have null curvature zones in the structure when only one static load test is applied. Alternatively, test data from multiple loading cases can be used in the static SSI (Bakhtiari-Nejad *et al*. 2005, Wang *et al*. 2012). In the case of bridges, static tests with multiple loading cases can be carried out by changing the location of truck loads. Apart from the importance of loading cases in the static SSI, the Optimal Sensor Placement (OSP) is also a vital issue. OSP has the potential to reduce life cycle costs of the structure considerably from an economic perspective (Liu *et al*. 2020). Also, good sensor configuration is the basis of accurate SSI result (Li *et al*. 2017). The OSP problem can be formulated as a combinatorial optimization problem aiming at minimizing or maximizing some objective functions with the sensor location vector being the design variable. Usually, these objective functions include some norms of the Fisher Information Matrix (FIM) (Li *et al*. 2012). Regarding the formidable dimension of real structures, seeking the OSP is an intractable task by ordinary global search methods because the size of the solution space is huge and the searching efficiency is low. For example, there are $C_n^{N_m}$ possible sensor placement configurations for a model with n DOFs and N_m sensors. For instance, the case of 70 DOFs and 20 sensors means $C_{70}^{20} = 1.6188 \times 10^{17}$ possible sensor placement configurations. Typically, the combinatorial optimization problem is a non-convex optimization problem. Existing static OSP methods (Sanayei *et al*. 2015, Sanayei and Chitra 2002) adopt the strategy of greedy algorithms to find a sub-optimal solution. During this process, a subset of sensors is either added or removed to improve some criteria regarding the OSP. The strategy of greedy algorithms has the problem of making these choices (adding or removing sensors) too early, preventing them from finding the best overall solution later. This is a typical problem for OSP method using greedy algorithm (Bertola *et al*. 2017). Another limitation is that these methods cannot specify the number of different types of sensors to be used while different types of sensors are adopted in real SSI applications. These methods only consider the total number of sensors but cannot control the number of inclinometers or deflection gauges.

To deal with these limitations, the objective of this

research includes (1) developing a static SSI method using multiple loading cases under the framework of MEMOM; (2) proposing a systematic method to determine the OSP configuration for static SSI under multiple loading cases. The organization of the paper is as follows: firstly, the procedure to implement SSI by MEMOM under multiple loading cases is presented. This starts with the previous method aimed for single loading case. Then, the procedure to combine the equations for different loading cases is described. In section 3, the property of the FIM is presented first. Then, the formulation of Genetic Algorithm based OSP using the FIM under multiple loading cases are illustrated. Section 4 provides two numerical examples to illustrate and validate the proposed methods in different typologies of structures. Finally, in section 5, some conclusions are drawn.

2. Methodology

2.1 SSI by MEMOM under single loading case

In SSI by MEMOM under single loading case (Lei *et al*. 2019), a finite element model (FEM) of the analyzed structure is required and its static equilibrium equations should be established as follows

$$[K]\{\delta\} = \{f\} \tag{1}$$

For 2D analysis, the stiffness matrix $[K]$ includes the element length L_j, elastic modulus E_j, area A_j, inertia I_j of element j (j = 1, 2, …, N_e, where N_e is the number of elements). The displacement vector $\{\delta\}$ includes the horizontal deflection u_i, vertical deflection v_i and rotation w_i of node i (i = 1, 2, …, N_n, where N_n is the number of nodes), while the force vector $\{f\}$ includes the horizontal force H_i, vertical force V_i and bending moment M_i applied on the nodes.

Since the main objective of SSI is to assess the structure condition, the estimations of axial stiffnesses and bending stiffnesses are of primary importance. Hence, this paper will focus on the structural mechanism involved with axial stiffnesses and bending stiffnesses. Different unknown stiffnesses may appear in the same column in the matrix [K]. In addition, in controlled static load tests, the magnitudes of the external force and the measured responses are known to engineers. To differentiate the knowns from the unknowns, those known elements are indicated by subscript 1 while those unknown elements are indicated by subscript 0. As unknown variables appear in the coefficient matrix in Eq. (1), a series of algebraic operations have to be applied on the equilibrium equations to formulate the observability equations (Lei *et al*. 2019), as shown in Eq. (2).

$$[B]\cdot\{z\} = \begin{bmatrix} K_{10}^* & 0 \\ K_{00}^* & -I \end{bmatrix}\begin{Bmatrix} \delta_0^* \\ f_0 \end{Bmatrix} = \begin{Bmatrix} f_1 - K_{11}^*\delta_1^* \\ -K_{01}^*\delta_1^* \end{Bmatrix} = \{D\} \tag{2}$$

In the observability equations, the coefficient matrix $[B]$ contains the measured displacements $\tilde{\delta}$ and the known element lengths (note that [B] is not equal to $\begin{bmatrix} K_{10}^* & 0 \\ K_{00}^* & -I \end{bmatrix}$, refer to Lozano-Galant *et al*. (2013)). The unknown vector $\{z\}$ (not equal to is $\begin{Bmatrix} \delta_0^* \\ f_0 \end{Bmatrix}$, refer to Lozano-Galant *et al*. (2013)), composed of three types of unknowns, including (1) single unknowns, such as bending stiffnesses EI_j and axial stiffnesses EA_j; (2) coupled unknowns, such as $EI_j w_i$ or $EI_j v_i$; (3) reactions (H_i, V_i, M_i). The right-hand-side vector {D} is composed of external nodal forces f_1 and internal nodal forces ($K_{11}^*\delta_1^*$, $K_{01}^*\delta_1^*$). The superscript * indicates algebraic operations (e.g., multiplication, division) that have been applied on the matrices or vectors, and for the details, please refer to Lozano-Galant *et al*. (2013).

Based on the observability equations, the observability (existence and uniqueness) of any unknown variables in the vector $\{z\}$ can be determined symbolically from the null space of the coefficient matrix $[B]$. In addition, a particular solution of the observability equation might be obtained numerically by least-square methods. This particular solution for those observable unknowns is regarded as the final estimation.

Despite its efficiency in determining the observability of the target parameters, the overall accuracy of this method is far from satisfactory when measurement errors exist. However, measurement errors are issues that must be addressed in any practical SSI application. Some improvements can be made to alleviate the adverse effect of measurement errors. For instance, the compatibility conditions (geometrical relations among nodal displacements) in beam-like structures can be obtained from the observability equations and can be used to smooth away the incompatibility induced by this kind of errors (Lei *et al*. 2018). Also, averaging the estimations from different combinations of rotation measurements might enable robust estimations of the target parameters. However, both methods suffer from the limitation in either the structure type or the measurement type. To have a more general method, the SSI by MEMOM is proposed. In the observability equations, the measured displacement $\tilde{\delta}$ contained in the coefficient matrix $[B]$ are separated into an error-free term $\hat{\delta}$ and an error term ϵ_δ. Then, the error terms ϵ_δ for all measured displacements are transferred to a new unknown vector $\{z_e\}$. In this way, a new observability equation with measurement errors included in the unknowns $\{z_e\}$ is formulated, as shown in Eq. (3) (For the details of $[B_e]$ and $[Z_e]$, please refer to Lei *et al*. 2019).

$$[B_e]\cdot\{z_e\} = \{D\} \tag{3}$$

In this new observability equation, the measured displacements $\tilde{\delta}$ are included in the coefficient matrix $[B_e]$. Compared to the unknown vector $\{z\}$ in Eq. (2), the new unknown vector $\{z_e\}$ also contains the error terms ϵ_δ. The Eq. (3) always has more unknowns than the number of equations. To solve this underdetermined system, other conditions have to be imposed. The discrepancy between the measured response and the predicted response can be minimized by numerical optimization. The objective function is the square sum of the ratios between the error

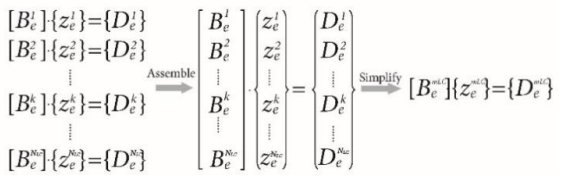

Fig. 1 Formulation of observability equations under multiple loading cases by stacking (*mLC* stands for multiple loading cases; N_{LC} is the number of loading cases)

terms and the measured displacements, as shown in Eq. (4)

$$f(z_e) = \sum_{i=1}^{Nm} \left(\frac{\epsilon_{\delta_i}}{\tilde{\delta}_i} \right)^2 \quad (4)$$

where $\tilde{\delta}_i$ is the value of the i^{th} measurement; ϵ_{δ_i} is the error term for δ_i. A step by step example of the whole process can be found in Lei *et al*. (2019).

2.2 SSI by MEMOM under multiple loading cases

To make use of multiple loading cases, the observability equations for different loading cases are obtained first and then assembled. The procedure to combine observability equations for different loading cases is illustrated in Fig. 1.

The superscript k in $[B_e^k]$, $\{z_e^k\}$ and $\{D_e^k\}$ indicates the equation is formulated from the k^{th} loading case. To obtain the final equation, all unknown vectors are concatenated together first. Then, the coefficient matrices are rearranged and assembled according the appearing order of variables in the concatenated unknown vector. It is assumed that the structure behaves linearly and structural parameters do not change during the static tests. This is to say, the unknown structural parameters appearing duplicately for different loading cases are the same. Hence, this system of equations can be simplified by merging the columns that are related to the same structural parameters.

In the final observability equations, the unknowns are composed of three types: (1) single unknowns, including structural parameters (bending/axial stiffnesses, EA_i, EI_i), reactions (H_i^k, V_i^k *or* M_i^k) from different loading cases, (2) coupled unknowns, products of structural parameters with unknown displacements from different loading cases ($EA_i u_i^k$, $EI_i v_i^k$) or products of structural parameters with error terms from different loading cases ($EI_i \epsilon_{u_i^k}$, $EI_i \epsilon_{v_i^k}$); (3) additional single unknowns that are obtained by the decoupling of the coupled unknowns and that are not included in the first type, such as the unmeasured displacements (u_i^k) and the error terms ($\epsilon_{v_i^k}$).

After obtaining the final observability equations, the structural parameters are estimated by minimizing the square sum of the ratios between the error terms and the measured displacements in all loading cases, as shown in Eq. (5).

$$f(z_e^{mLC}) = \sum_{k=1}^{N_{LC}} \sum_{j=1}^{N_m} \left(\frac{\epsilon_{\delta_j^k}}{\tilde{\delta}_j^k} \right)^2 \quad (5)$$

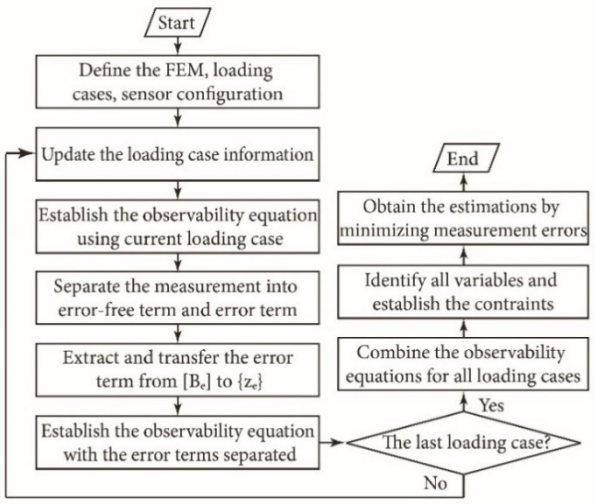

Fig. 2 Flowchart of the structural system identification by measurement-error minimizing observability method under multiple loading cases

where $\tilde{\delta}_j^k$ is the value of the j^{th} measurement in the k^{th} loading case; $\epsilon_{\delta_j^k}$ is the error term for $\tilde{\delta}_j^k$.

The flowchart of the procedure to carry out SSI by MEMOM under multiple loading cases is summarized in Fig. 2.

3. Genetic algorithm based optimal sensor placement

The genetic algorithm (GA) based optimal sensor placement (OSP) relies on the maximization of the norm of the Fisher Information Matrix (FIM). In section 3.1, the property of the FIM regarding its application in OSP is discussed. Existing research on the OSP for static SSI is reviewed and some limitations are pointed out. Subsequently, the formulations of the FIM for both single loading case and multiple loading cases are presented. The advantage of the GA-based OSP method and its implementation as well as a flowchart of the proposed procedure is presented at the end of this section.

3.1 Existing research on OSP for static SSI

The objective of OSP is to find the best sensor configuration to extract as much information from the structural response as possible when the number and type of sensors are assumed. The OSP for static SSI can be stated as maximizing or minimizing an objective function, where the design variable is the sensor location vector $\{\Theta\}$ and the constraint is the number of available sensors and type (inclinometers and deflectometers). Current research dealing with sensor placement mainly focuses on the OSP for dynamic SSI (Li *et al*. 2017, Meo and Zumpano 2005, Tong *et al*. 2014). In fact, little attention has been paid to the static case. Existing research on the OSP for static SSI is mainly based on the FIM $[F]$ (Sanayei *et al*. 2015, Sanayei and Chitra 2002). The rationale of this sensor placement method is based on the Cramér-Rao lower bound, which is

presented as follows

$$\mathrm{E}\left[\left(\hat{\theta}(D)-\theta\right)\left(\hat{\theta}(D)-\theta\right)^{T}\right] \geq [F^{-1}] \tag{6}$$

Here, the superscript -1 indicate the inverse of a matrix. The Cramér-Rao lower bound shows that the inverse $[F^{-1}]$ of the FIM lower bounds the error covariance matrix for any unbiased estimator $\hat{\theta}(D)$ of the parameter vector θ using data *D*. Hence, maximization of the norms of the matrix $[F]$ would yield a possible minimum lower bound of the covariance of the estimation θ. Common norms of the matrix $[F]$ include trace, determinant and minimum singular values. Li *et al*. (2012) pointed out that different matrix norms were equivalent in the sense that one norm can be always bounded in a range by another norm with appropriate constant scaling factors. Hence, in this work, the determinant of the FIM, $det([F])$ is adopted as the objective function to judge the goodness of a sensor placement configuration. This is the most common criterion in current static OSP methods (Bakhtiari-Nejad *et al*. 2005, Sanayei *et al*. 2015, Sanayei and Chitra 2002).

In (Sanayei *et al*. 2015, Sanayei and Chitra 2002), the OSP was determined by gradually removing the sensors of low contribution to the determinant of the FIM from the initial sensor candidate set until the remaining number of sensors in the sensor candidate set is the same as the predefined number. Specifically, the determinant of the FIM using all remaining sensors was denoted by $det([F_0])$. The determinant of the FIM using all remaining sensor candidates excluding the i^{th} DOF was denoted by $det([F_{-i}])$. Then, the contribution of the i^{th} DOF was evaluated by the ratio $R_{Di} = det([F_{-i}]) / det([F_0])$. The higher R_{Di}, the less important the measurement of the i^{th} DOF. Then, the DOF with the highest R_{Di} (lowest importance) was removed from the initial sensor set. In this approach, one bad sensor was removed each time. In (Bakhtiari-Nejad *et al*. 2005), the importance of DOFs was also determined by the ratio R_{Di}. However, the R_{Di} was calculated only once using the initial sensor candidates. Then, all DOFs were sorted according to their importance index R_{Di}. The batch of sensors with low R_{Di} (high contribution) were selected for the OSP. Both methods evaluate the importance of potential sensor locations by checking the decrease in the determinant of the FIM after removing one DOF. The problem of this approach is that the non-linear and dependent nature of the interaction between sensor locations on the determinant of the FIM cannot be addressed due to the limitation of evaluating the importance of different DOFs separately. Furthermore, the sensor configurations for different loading cases were selected independently in Bakhtiari-Nejad *et al*. (2005). Consequently, the sensor locations vary in different loading cases. This leads to additional costs in the disassembly and the installation of sensors. Also, the number of deflectometers and inclinometers cannot be specified in these methods, only the sum of them. This means that these methods cannot well consider the available number and type of sensors.

3.2 Formulation of FIM under multiple loading cases

Firstly, the computation of FIM under single loading case $[F_s]$ (Lei *et al*. 2019) is given below.

$$[F_s(\Theta)] = [S(\Theta)^T][\Psi_0^2]^{-1}[S(\Theta)] \tag{7}$$

The FIM $[F_s]$ is composed of a sensitivity matrix $[S(\Theta)]$ and a noise variance matrix $[\Psi_0^2]$. The sensitivity matrix $[S(\Theta)]$ describes the effects of the variation of structural parameters on the selected measurements. This matrix has N_m rows and N_p columns, where N_m is the number of measurements (such as deflections or rotations) and N_p is the number of parameters (such as axial stiffnesses or bending stiffnesses). The noise variance matrix $[\Psi_0^2]$ of the measurements are typically available to engineers through instrument calibration, sensor-supplier information and engineering judgement (Bertola *et al*. 2017, Sanayei *et al*. 2015). The sensor location vector $\{\Theta\}$ is a binary vector with the length of N_d, where N_d is the number of DOFs in the model. Each element of the sensor location vector $\{\Theta\}$ is associated with one DOF. When the i^{th} DOF is measured, then $\Theta_i = 1$. Otherwise, $\Theta_i = 0$.

To obtain the sensitivity matrix $[S(\Theta)]$ for the measured DOF, the sensitivity matrix $[S^a]$ for all DOFs is obtained in terms of partial derivatives, as shown below

$$[S^a] = \frac{\partial \delta}{\partial \theta} = \frac{\partial\left[[K(\theta)^{-1}]\{f\}\right]}{\partial \theta} \tag{8}$$

where $\{f\}$ is the load vector for the single loading case. Note that the product of the matrix $[K]$ and its inverse $[K^{-1}]$ is an identity matrix. In addition, the partial derivative of any constant matrix with respect to any variable is zero. Hence, the following equation holds

$$0 = \frac{\partial[K \cdot K^{-1}]}{\partial \theta} = [K] \cdot \frac{\partial[K(\theta)^{-1}]}{\partial \theta} + \frac{\partial[K(\theta)]}{\partial \theta} \cdot [K^{-1}] \tag{9}$$

Combining Eq. (8) and Eq. (9), $[S^a]$ is given by

$$[S^a] = -[K(\theta)^{-1}]\frac{\partial[K(\theta)]}{\partial \theta}[K(\theta)^{-1}]\{f\} \tag{10}$$

The sensitivity matrix $[\mathrm{S}(\Theta)]$ for the selected measurements is obtained by extracting the associated rows of the matrix $[\mathrm{S}^{\mathrm{a}}]$ where the elements of $\{\Theta\}$ are equal to 1. Sanayei *et al*. (2015) pointed out that the noise variance matrix $[\Psi_0^2]$ was semi-definite and thus could be expressed in terms of a lower triangular matrix [L] and its conjugate transpose $[\mathrm{L}^{\mathrm{T}}]$ using the Cholesky decomposition

$$[\Psi_0^2] = [L] \cdot [L^T] \tag{11}$$

Substituting Eq. (11) into Eq. (7), then

$$\begin{aligned}[F_s(\Theta)] &= [S(\Theta)^T]([L] \cdot [L^T])^{-1}[S(\Theta)] \\ &= \left[\tilde{S}(\Theta)^T\right][\tilde{S}(\Theta)]\end{aligned} \tag{12}$$

and

$$\left[\tilde{S}(\Theta)\right] = [L^{-1}S(\Theta)] \tag{13}$$

By this way, the modified sensitivity matrix $[\tilde{S}(\Theta)]$ incorporates measurement uncertainty into the sensitivity matrix. With the formulation of FIM under one loading case, the procedure to obtain the FIM for a static load test comprised of N_{LC} loading cases is presented below.

Step 1: For the i^{th} loading case, obtain the sensitivity matrix $[S_i^a]$ for all DOFs using Eq. (10) and the lower triangular matrix $[L_i]$ from the noise variance matrix $\left[\Psi_{0,i}^2\right]$. Then, the modified sensitivity matrix $[\tilde{S}_i^a]$ for the i^{th} loading case is given by

$$\left[\tilde{S}_i^a\right] = [L_i^{-1}][S_i^a] \tag{14}$$

Step 2: Formulate the modified sensitivity matrix $\left[\tilde{S}_m^a\right]$ for all DOFs under multiple loading cases by combining the modified sensitivity matrices $[\tilde{S}_i^a]$ from different loading cases.

$$\left[\tilde{S}_m^a\right] = \begin{bmatrix} \tilde{S}_1^a \\ \vdots \\ \tilde{S}_{N_{LC}}^a \end{bmatrix} \tag{15}$$

Note that the modified sensitivity matrix $[\tilde{S}_m^a]$ for multiple loading cases has $N_{LC} \times N_d$ rows and N_p columns.

Step 3: Extracting the rows of the matrix $\left[\tilde{S}_m^a\right]$ where the corresponding DOFs are measured to formulate the modified sensitivity matrix $[\tilde{S}_m(\Theta_m)]$ for the selected DOFs under multiple loading cases.

The sensor placement vector $\{\Theta_m\}$ for multiple loading cases has $N_{LC} \times N_d$ elements. From a practical point of view, it is rational to keep the same sensor configuration in each loading case so that the cumbersome disassembly and installation of sensors due to the difference of sensor configurations can be avoided. Hence, the sensor placement vector $\{\Theta_m\}$ under multiple loading cases can be reduced to the case of the sensor placement vector $\{\Theta\}$ under one loading case while the information from multiple loading cases can be considered at the same time. This is also beneficial due to the reduction of the search space in the optimization regarding the computation aspect.

Step 4: Calculate the FIM for multiple loading cases, as shown in Eq. (16).

$$F_m(\Theta) = \tilde{S}_m(\Theta)^T \tilde{S}_{\mathrm{m}}(\Theta) \tag{16}$$

The modified sensitivity matrix $[\tilde{S}_{\mathrm{m}}(\Theta)]$ for the measured DOFs is obtained by extracting the associated rows of the matrix $[\tilde{S}_m^a]$ (Eq. (15)) where the corresponding DOFs are measured. The matrix $[\tilde{S}_{\mathrm{m}}(\Theta)]$ has $N_{LC} \times N_m$ rows and N_p columns. The FIM $F_m(\Theta)$ for multiple loading cases is a square matrix with N_p rows.

3.3 Optimal sensor placement using genetic algorithm

The mathematical formulation of the OSP problem for multiple loading cases is given below.

$$\Theta_{opt} = \max_{\Theta} det\ (F_m(\Theta)) \tag{17}$$

Subjected to the following constraints

$$N_{LC} \cdot \sum_{i \in v} \Theta_i = N_v \quad \Theta_i \in \{0,1\} \tag{18}$$

$$N_{LC} \cdot \sum_{j \in w} \Theta_j = N_w \quad \Theta_j \in \{0,1\} \tag{19}$$

where $F_m(\Theta)$ is the FIM determined by Eq. (16). N_v is the number of deflection measurements. N_w is the number of rotation measurements. Note that the imposition of constraints (18) and (19) enables the engineer to consider the factual situation about the available amount as well as the available types of sensors.

Current OSP methods for static SSI (Bakhtiari-Nejad *et al*. 2005, Sanayei *et al*. 2015, Sanayei and Chitra 2002) cannot address the nonlinear and dependent nature of the interaction between different sensor locations. This issue can be alleviated by heuristic and metaheuristic algorithms (Zhou *et al*. 2015), such as Genetic Algorithm (GA), particle swarm optimization (Tan and Zhang 2019) or microhabitat frog-leaping algorithm. In this paper, the GA proposed by Deep *et al*. (2009) is used to solve the combinatorial optimization problem for the OSP. In this algorithm, the optimization process includes (1) initialization stage; (2) evaluation stage; (3) selection stage; (4) crossover stage; (5) mutation stage; (6) truncation stage. In stages (1) and (2), random feasible solutions will be generated and evaluated using the fitness functions, which are the same as the objective function. Then, the selection, crossover, mutation and truncation stages are carried out repeatedly. This first three stages aim at updating and diversifying the solutions while the truncation stage aims at satisfying the applied constraints (e.g., Eqs. (19) and (20)) and the integer restriction on Θ_i. By this mean, many groups of solutions are obtained and evaluated using the fitness function. The best solution among the current group and its fitness value are recorded and compared with the best ones from the previous groups. If the desired convergence accuracy is met or the predefined iteration number is reached, the algorithm will terminate and the recorded best solution is determined as the final solution. For more details, please refer to Deep *et al*. (2009).

The procedure for the GA-based OSP is summarized as the 8 steps described below and its flowchart is depicted in Fig. 3. The FIM for the structure subjected multiple static loading cases is formed in steps 1-6 while the OSP is solved using the GA in steps 7 and 8.

Step 1: Define the FEM and the loading cases of the concerned structure.

Step 2: Update the i^{th} loading case information.

Step 3: Calculate the sensitivity matrix $[S_i^a]$ for the i^{th} loading case with Eq. (10).

Step 4: Form the modified sensitivity matrix $[\tilde{S}_i^a]$ for the i^{th} loading case with Eq. (14).

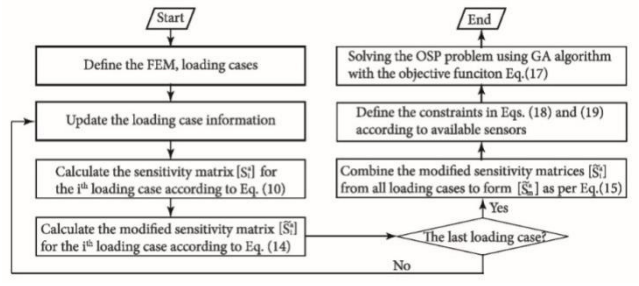

Fig. 3 Flowchart of the genetic algorithm based optimal sensor placement method

Step 5: Check whether this is the last loading case. If yes, go to step 6; otherwise, repeat steps 2-4.

Step 6: Form the modified sensitivity matrix $[\tilde{S}_m^a]$ for all DOFs using Eq. (15).

Step 7: Prepare the constraints according to available number and type of sensors;

Step 8: Solve the OSP problem using the GA.

4. Numerical examples

To verify the effectiveness of the proposed method, two structures subjected to static loading are studied numerically. The first one relates to a 3-span continuous bridge and the second one relates to a floor beam in a high-rise frame. For these examples, the interested parameters are identified using one loading case and two loading cases, respectively. The total number of different types of sensors for these two cases are kept the same. First, the sensor locations in two examples are determined by the GA-based OSP method. Note that the loading position is also an important factor to affect the accuracy of the identification. In this work, the loading positions were designed based on the bending curve of the structure and the target stiffness parameters to be identified. Then, the problem of identifying all parameters using single loading case is illustrated. Finally, the advantage of using multiple loading cases is presented and more useful information could be provided. In real case, it is difficult to carry out impose the static loads of all cases at the same time. Furthermore, there may be not so much loading tools (e.g., loading trucks).

As the purpose of the paper is to settle the theoretical basis and the benefits of the proposed method some engineering assumptions has been made at this stage: a) modelling error is not considered, as it is wanted to study the effects of measurement errors isolated; b) load tests, which are done with heavily loaded trucks, are not modeled with point loads acting on their axles but as uniformed loads; c) to improve accuracy, the number of measurements was higher than the number of unknown parameters to be identified.

In these examples, FEMs are used to obtain displacements in the nodes for different loading cases. Proportional noise is added to these displacements to generate measurement sets, as shown by Eq. (20).

$$\tilde{\delta} = \delta_r \cdot (1 + E_{level} \cdot \xi) \tag{20}$$

where δ_r are the displacements calculated from FEMs, E_{level} is the value of the proportional error and ξ is a random number following normal distribution with mean of 0 and standard deviation of 0.5.

4.1 Example 1: 3-span continuous bridge

The first example is a 36 m + 54 m + 36 m continuous bridge. The FEM and its parameterization are depicted in Fig. 4. This FEM is composed of 43 nodes and 42 beam elements. As the continuous bridge is mainly excited by its bending behavior, the parameters to be estimated in this structure are the 14 bending stiffnesses. To identify these parameters, the candidate measurements are the 39 deflections v and 43 rotations w in this structure.

The theoretical values of the bending stiffnesses for the first span ($EI_1 - EI_4$), those for the second span ($EI_5 - EI_{10}$) and those for the third span ($EI_{11} - EI_{14}$) are equal to $1.5\times107\ kN\cdot m^2$, $2.5\times107\ kN\cdot m^2$ and $1.5\times107\ kN\cdot m^2$, respectively. Four loading cases are adopted. Uniform loads of q = 20 kN/m are applied over different regions of the continuous bridge. The ranges of the applied load for the four loading cases together with the bending moment diagram are shown in Fig. 5.

In this example, five scenarios are studied. Their loading

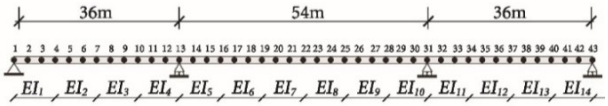

Fig. 4 Finite element model for the 36 m + 54 m + 36 m continuous bridge

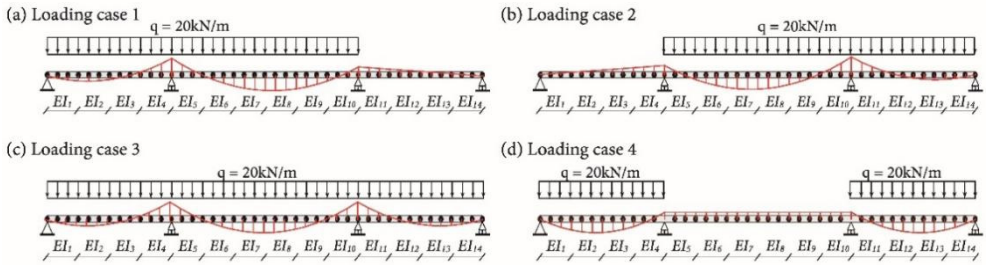

Fig. 5 Loading cases and associated bending moment diagrams for: (a) LC1 (b) LC2 (3) LC3 (4) LC4

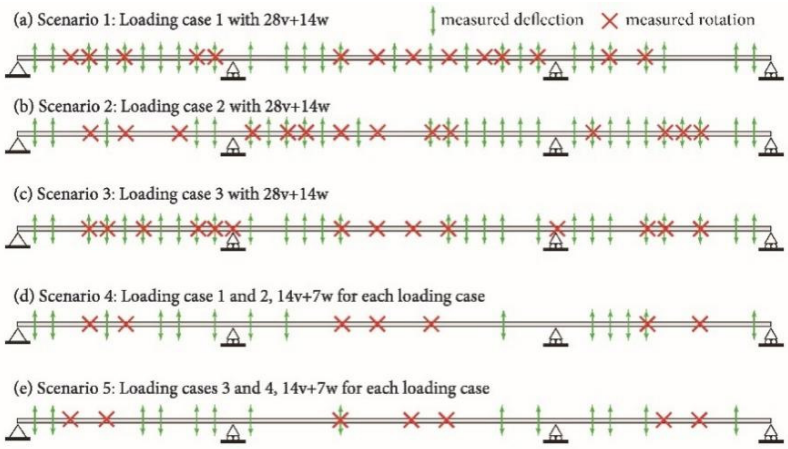

Fig. 6 Locations of the measured deflections (v) and rotations (w) for different scenarios: (a) scenario 1; (b) scenario 2; (c) scenario 3; (d) scenario 4; (e) scenario 5

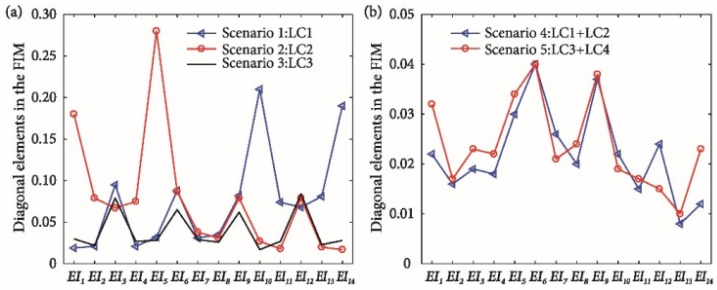

Fig. 7 Diagonal elements of the inversed Fisher information matrix for (a) scenarios 1-3; (b) scenarios 4 and 5

cases and sensor configurations are depicted in Fig. 6. The 14 bending stiffnesses are estimated using one loading case (LC1-LC3) in scenarios 1-3 while this is done by using two loading cases in scenarios 4 (LC1+LC2) and 5 (LC3+LC4). In scenarios 1-3, it is assumed that 28 deflections v and 14 rotations w are measured to identify these 14 bending stiffnesses. In each loading case in scenarios 4 and 5, 14 deflections and 7 rotations are used, summing up to 28 deflections and 14 rotations for the associated scenario. The scenarios 1-3 are used to show that the bending stiffnesses of some local regions cannot be identified using single loading case. The last 2 scenarios are used to show the advantage and effectiveness of using multiple loading cases.

Due to the existence of null curvature zones, some parameters cannot be identified using only one loading case. As indicated by Eq. (6), the terms in the diagonal of the inversed FIM $[F^{-1}]$ are lower bounds of the parameter variances (Sanayei *et al*. 2015). Large values in diagonal elements of $[F^{-1}]$ indicate unidentifiable parameters. The diagonal elements of the inversed FIM $[F^{-1}]$ associated with scenarios 1-3 are illustrated in Fig. 7(a).

From this figure, it is anticipated that the bending stiffnesses EI_{10} and EI_{14} cannot be identified in scenario 1, and the bending stiffnesses EI_1 and EI_5 cannot be identified in scenario 2. Hence, an absolute bound of [0.5, 1.5] is applied on the normalized estimation of these unidentifiable parameters in the optimization. In the case of scenario 3, the diagonal elements of the inversed FIM, $[F^{-1}]$, for the bending stiffnesses $EI_1 - EI_{14}$ are all smaller than 0.1 (Fig. 7(a)). However, the extent of variation of EI_3, EI_6, EI_9 and EI_{12} is much higher than that of other parameters. In Fig. 7(b), the diagonal elements of the inversed FIM for all parameters in scenarios 4 and 5 are always smaller than 0.05. This indicates a possible good estimation of all bending stiffnesses. Hence, no bound is applied on any parameter estimation in scenarios 4 and 5.

For each OSP configuration of the associated scenario, 200 measurement sets are simulated using Eq. (20) with the proportional error of 5%. The result of the estimations of the bending stiffnesses in each scenario is summarized by the boxplots in Fig. 8.

The boxplot shows the first quartile Q_1 and the third quartile Q_3 of the estimations as the top and the bottom of the box and the median is shown by the red line inside the box. The red crosses are the estimates that deviates most from the rest of the estimates. The longer the box, the higher the dispersion in the estimations. From Fig. 8, a clear connection between the dispersion of the estimations and the extent of curvature is observed. In scenario 1 (Fig. 8(a)), large variations in the estimation of the parameters (EI_{10} and EI_{14}) for null curvature zones are observed despite the applied absolute bound of [0.5, 1.5] on the normalized values of the estimations. Hence, the dispersion of these estimations cannot be reduced by imposing these bounds. Similar problem is observed for the bending stiffnesses EI_1 and EI_5 in scenario 2 (Fig. 8(b)).

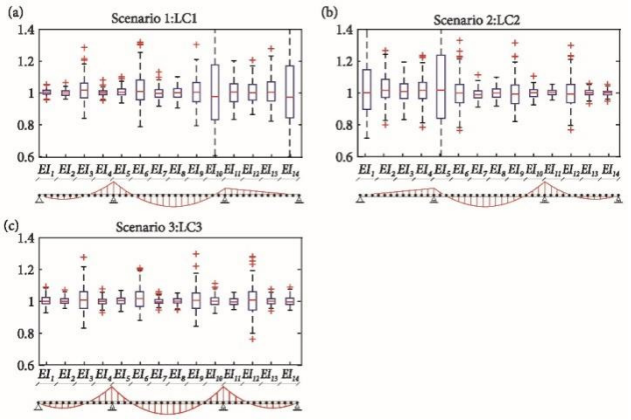

Fig. 8 Boxplot of the 200 estimations for EI_1-EI_{14} in scenarios 1-3

The extent of the dispersion in scenario 3 is less than those in scenarios 1 and 2. The averaged Coefficients of Variation (C.O.V.s) of the bending stiffnesses $EI_1 - EI_{14}$ for the five scenarios are given in Table 1. It is seen that the averaged C.O.V.s of the parameters in scenario 3 is the half of those in scenarios 1 and 2. This is because the loading case in scenario 3 excites the bending behavior of the whole structure more than those in scenarios 1 and 2. However, the curvature of the zones adjacent to the inflection points in the bending moment diagram for LC3 (Fig. 8(c)) is still quite low. As a result, the dispersion in EI_3, EI_6, EI_9 and EI_{12} is comparatively high. The corresponding C.O.V.s for these parameters in scenario 3 are 0.080, 0.074, 0.071, 0.088, while the C.O.V.s for the remaining p

arameters ranging between 0.017 and 0.031.

The boxplot of the 200 estimations for $EI_1 - EI_{14}$ in scenarios 4 and 5 is given in Fig. 9. The range of y-axis in Fig. 9 is set the same as that in Fig. 8 to ease the comparison between the dispersion of the estimations in different scenarios. From this figure, it is seen that when multiple loading cases are used, all flexural stiffnesses can be identified and the dispersion in the estimations are much less than that in scenarios 1-3 (Fig. 8).

A comparison of the C.O.V.s for all parameters obtained from scenarios 3-5 is depicted in Fig. 10. As the objective function in Eq. (17) aims to reduce the overall variance in all parameters, the optimization algorithm mainly tries to reduce the large variance in estimations for bending stiffnesses with null curvatures (i.e., EI_3, EI_6, EI_9 and EI_{12} in scenario 3) while keeping the slight increase of the sum of the variance in the estimations for other bending

Table 1 The averaged Coefficients of Variation (C.O.V.s) of the estimations of $EI_1 - EI_{14}$ in scenarios 1-5

Scenario	Loading case	averaged C.O.V.s
1	1	0.082
2	2	0.079
3	3	0.040
4	1+2	0.032
5	3+4	0.031

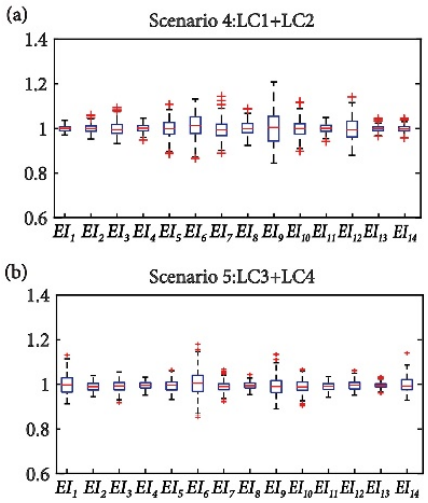

Fig. 9 Boxplot of the 200 estimations for $EI_1 - EI_{14}$ in scenarios 4 and 5

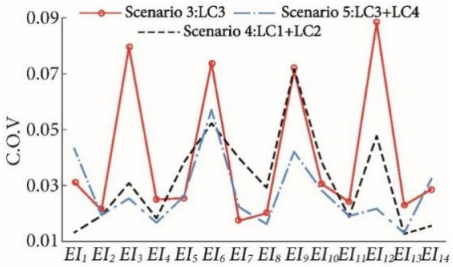

Fig. 10 Comparison of the C.O.V.s for the estimations of $EI_1 - EI_{14}$ in Scenarios 3, 4 and 5

stiffnesses.

The averaged C.O.V.s for all bending stiffnesses (Table 1) is reduced from 0.040 in scenario 3 to 0.032 in scenario 4. The decrease of the averaged C.O.V.s for all parameters is mainly due to the decrease of the C.O.V.s for EI_3, EI_6 and EI_{12}. In Fig. 10, the C.O.V.s for EI_3, EI_6 and EI_{12} are reduced from 0.080, 0.074, 0.088 in scenario 3 (LC3) to 0.031, 0.052, 0.048 in scenario 4 (LC1+LC2), respectively, while the C.O.V.s for EI_9 in scenarios 3 (0.071) and 4 (0.072) does not change much. For the remaining parameters, the C.O.V.s for EI_1, EI_{13}, EI_{14} decrease drastically while the C.O.V.s in EI_5, EI_7, EI_8 and EI_{10} increase from 0.026, 0.017, 0.020, 0.031 to 0.038, 0.040, 0.029, 0.038, respectively.

In scenario 5, the averaged C.O.V.s for all bending stiffnesses is 0.031. The dispersion of all parameters is controlled to an acceptable level ranging between 0.013 and 0.056. The C.O.V.s for the bending stiffnesses associated with null curvature zones, namely EI_3, EI_6, EI_9 and EI_{12} decreased from 0.080, 0.074, 0.071, 0.088 to 0.025, 0.057, 0.042, 0.022, corresponding with reductions of 68%, 23%, 41% and 75%, respectively. Despite the increase of C.O.V.s in EI_1(38%), EI_7(29%) and EI_{14}(10%), the reductions of the C.O.V.s in the remaining parameters are at least 20%.

Overall, it is seen that loading case 3 performs better than loading cases 1 and 2. This is because that in case 3,

more loadings was applied, which will provide more effective information for system identification, and makes the uncertainty also reduced as shown in Table 1. As mentioned, for case 1, case 2 and case 3, which correspond to scenario 1, scenario 2, and scenario 3, respectively, they are all single loading cases. The multiple loading cases can be seen in scenario 4 and scenario 5, and from these figures, it is found the extend of variation and the COV of the stiffness parameters reduce compared with the ones in signal load scenarios. This provides evidence that the multiple loading cases have better performance.

In summary, from the analysis above, it is seen that after applying multiple loading cases: (a) the bending stiffnesses associated with null curvature zones in one loading case can be effectively identified; (b) the overall variance in the estimations of all bending stiffnesses can be significantly reduced by using multiple loading cases; (c) the combination of different loading cases has beneficial impact on the accuracy of the estimations.

4.2 Example 2: A floor beam in a high-rise frame

In this section, the proposed method will be illustrated by a floor beam in a high-rise frame structure. In a previous study on the identification of a floor beam in a 13-story frame (Lei *et al*. 2019), it was found that the bending stiffnesses of null curvature zones cannot be identified. In this example, those unidentifiable parameters are investigated by the proposed SSI by MEMOM using multiple loading cases.

The FEM of this structure and its parameterization is depicted in Fig. 11(a). It has 111 nodes and 158 elements. The whole FEM is parameterized by 15 bending stiffnesses and 15 axial stiffnesses. The objective is to identify the bending stiffnesses of the selected floor beam depicted in Fig. 11(a). This floor beam is parameterized by seven bending stiffnesses, $EI_{1f} - EI_{7f}$ and seven axial stiffnesses, $EA_{1f} - EA_{7f}$. The values of the areas and inertias of the remaining regions (Fig. 11(a)) are presented in Table 2. The values of $EA_{1f} - EA_{7f}$ EI_{2f}, EI_{3f} and $\mathrm{EI}_{5\mathrm{f}} - \mathrm{EI}_{7\mathrm{f}}$ are assumed to be the same as type VIII in Table 2 while stiffness reductions of 40% and 30% are applied on EI_{1f} and EI_{4f}, respectively, to simulate the effects of structural damages. The elastic modulus E of all elements is 3.5×10^4 MPa.

Table 2 Values of the parameters for the high-rise frame (Note: A for area and I for inertia)

Regions	A (m^2)	I (m^4)
I	0.563	0.026
I	0.360	0.011
III	0.250	0.005
IV	0.360	0.011
V	0.250	0.011
VI	0.160	0.002
VII	1.800	5.400
VIII	0.180	0.005

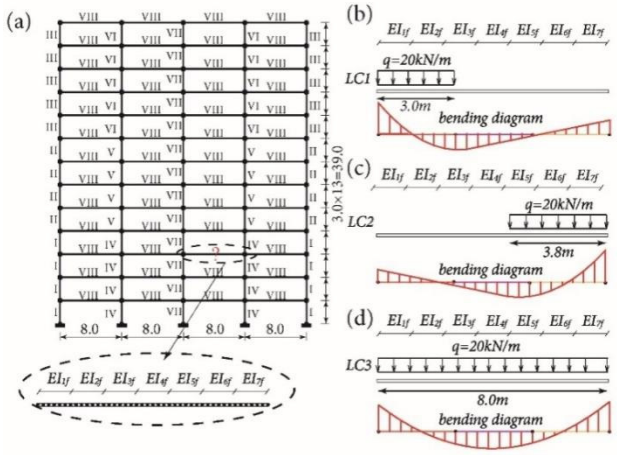

Fig. 11 (a) Finite element model of the 13-story frame structure with the targeted beam to be identified (Unit: m); (b) loading case 1(LC1) and its bending moment diagram; (c) loading case 2(LC2) and its bending moment diagram; (d) loading case 3(LC3) and its bending moment diagram

Three loading cases (LC1-LC3) are studied. Uniform loads of 20 kN/m are introduced into different parts of the floor beam in LC1-LC3. The range of these loading cases and the bending moment diagrams are shown in Figs. 11(b)-(d). All the 15 axial and 15 bending stiffnesses are assumed as unknown. As deflections v and rotations w are only measured within the target floor beam, it is anticipated that only $EI_{1f} - EI_{7f}$ can be estimated. However, this does not guarantee the accuracy of the parameter estimation when only one loading case is adopted, as shown below.

To demonstrate the advantage and effectiveness of using multiple loading cases, scenarios 1-4 are considered, as depicted in Fig. 12. It is assumed that 34 deflections and 16 rotations are used to identify $EI_{1f} - EI_{7f}$. The first three scenarios aim to identify the bending stiffnesses under one loading case from LC1-LC3. Scenarios 4 aims to improve the estimations by using LC1 and LC2 together. In both loading cases, 17 deflections and 8 rotations are used, summing up to 34 deflections and 16 rotations for the associated scenario. It should be noted that these number of

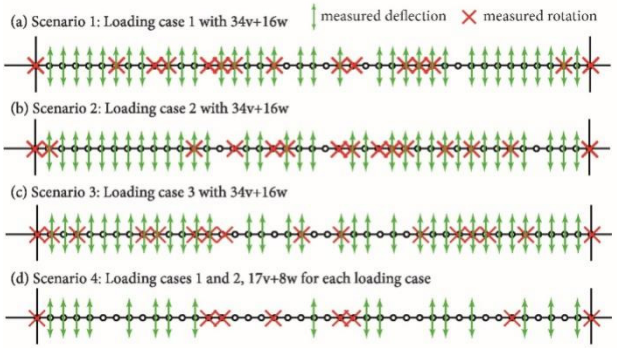

Fig. 12 Locations of the measured deflections (v) and rotations (w) for different scenarios: (a) scenario 1; (b) scenario 2; (c) scenario 3; (d) scenario 4

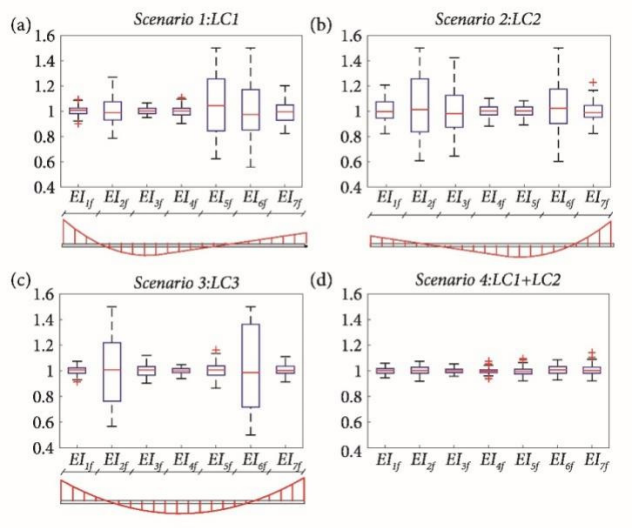

Fig. 13 Box plots of the estimations of different scenarios: (a) Scenario 1; (b) Scenario 2; (c) Scenario 3; (d) Scenario 4

sensors are adopted here to improve the accuracy of the estimations. Minimum number of sensors is the number of parameters to identify. The final sensor configurations for these scenarios are depicted in Fig. 12.

During the optimization, the absolute constraints of [0.5, 1.5] are applied on the bending stiffnesses for the null curvature zones, namely, LC1 (EI_{2f}, EI_{5f}, EI_{6f}), LC2 (EI_{2f}, EI_{3f} EI_{6f}) and LC3 (EI_{2f}, EI_{6f}). When LC1 and LC2 are used together, all the diagonal entries of the inversed FIM are lower than 0.05. Hence, all bending stiffnesses can be identified and no constraint is applied on them in scenario 4. For each OSP configuration of the associated scenario, 200 measurement sets are simulated using Eq. (20) with an error level of 5%. The 200 estimations of the 14 bending stiffnesses are summarized by the boxplots in Fig. 13.

All the y axes are scaled to [0.4, 1.6] to ease the comparison between different scenarios. In scenario 1-3 (Figs. 13(a)-(c)), single loading cases are used to obtain the estimations of the bending stiffnesses. The estimations of bending stiffnesses associated with null curvature zones have much larger dispersion (indicated by the length of the box) than other bending stiffnesses. In scenario 4 (Fig. 13(d)), it is seen that the dispersion of all parameters is well controlled when compared with those for scenarios 1-3. In the meanwhile, the dispersion of the estimations of bending stiffnesses associated with zones of high curvatures is also reduced obviously.

The averaged C.O.V.s for scenarios 1-4 are 0.122, 0.11, 0.114 and 0.029, respectively. Drastic decrease is observed in scenario 4. For each of the bending stiffnesses $EI_{1f} - EI_{7f}$, the lowest C.O.V.s from scenarios 1-3 are 0.031, 0.098, 0.026, 0.022, 0.042, 0.201, 0.041 while the associated C.O.V.s in scenario 4 are 0.024, 0.031, 0.021, 0.023, 0.031, 0.035, 0.039, respectively. This means decreases of 22.6%, 68.4%, 19.2%, -4.5%, 26.2%, 82.6%, 4.9% for these parameters. Despite of the slight increase of C.O.V. for EI_{4f}, the overall results are significantly improved.

It should be pointed out that the uniform loading was adopted in examples 1 and 2 to settle a theoretical basis for the proposed method. Concentrated loading and experimental study will be carried out in the future study.

5. Conclusions

This paper presents the static Structure System Identification (SSI) by Measurement Error-Minimizing Observability Method (MEMOM) under multiple loading cases for first time in the literature. The observability equations for different loading cases are concatenated together so that the information from multiple loading cases can be addressed simultaneously. The estimations of the parameters are determined by minimizing the square sum of the ratios between the error terms and the measured displacements. The method presented here is an improvement on the SSI by MEMOM under single loading case regarding its ability to identify those parameters in null curvature zones.

In the meanwhile, the Optimal Sensor Placement (OSP) problem for the static SSI is formulated as a combinatorial optimization problem with the determinant of the Fisher Information Matrix as the objective function and the sensor location vector as the design variable. The location of the sensors in each loading case is kept as a constant to avoid the cumbersome work of the disassembly and the installation of sensors. Also, the number of measured deflections and rotations can be specified directly.

To justify the effectiveness of the proposed methods on beam and frame like structures the numerical examples of a 3-span continuous bridge and a 13-storey frame are investigated using noisy measurements with respect to the loading cases and measurement types. The numerical results show the capability of the proposed method to improve the estimations of unidentifiable parameters due to the limitations of using only single loading case. After using multiple loading cases, the overall estimation accuracy and dispersion can be improved significantly. In addition, the proposed GA-based OSP method could give reasonable results for the SSI and it provides a systematic way to design sensor configuration under multiple static loading cases. In the future work, the verification of the proposed GA-based OSP method based on multiple static loading cases and a single case with the same sensor locations will be studied to further illustrate the advantage of this method.

Acknowledgments

This work was partially funded by the Scientific Research Fund of Institute of Engineering Mechanics, China Earthquake Administration (Grant No. 2019 EEEVL0401); Natural Science Foundation of Shenzhen (Grant No: JCYJ20190806143618723); Spanish Ministry of Economy and Competitiveness and FEDER fund (Grant No: BIA2017-86811-C2-1-R, directed by José Turmo, and Grant No: BIA2017-86811-C2-2-R). Authors are also

indebted to the Secretaria d' Universitats i Recerca de la Generalitat de Catalunya for the funding provided through Agaur (Grant No: 2017 SGR 1481). Part of this work was done through a collaborative agreement between Tongji University (China) and Technical University of Catalonia, UPC. The financial support from the Chinese High-End Foreign Experts program (GDW20143100115) is greatly appreciated. Funding for this research has been provided to Jun Lei by the Chinese Scholarship Council through its program No.201506260116 and by the Spanish Ministry of Economy and Competitiveness through its program BES-2014-07022 for his PhD stays.

References

Abdo, M.A.-B. (2012), "Parametric study of using only static response in structural damage detection", *Eng. Struct.*, **34**, 124-131. https://doi.org/10.1016/j.engstruct.2011.09.027

Bakhtiari-Nejad, F., Rahai, A. and Esfandiari, A. (2005), "A structural damage detection method using static noisy data", *Eng. Struct.*, **27**(12), 1784-1793. https://doi.org/10.1016/j.engstruct.2005.04.019

Banan, M.R., Banan, M.R. and Hjelmstad, K.D. (1994a), "Parameter estimation of structures from static response. II: Numerical simulation studies", *J. Struct. Eng.*, **120**(11), 3259-3283. https://doi.org/10.1061/(ASCE)0733-9445(1994)120:11(3259)

Banan, M.R., Banan, M.R. and Hjelmstad, K.D. (1994b), "Parameter estimation of structures from static response. I. Computational aspects", *J. Struct. Eng.*, **120**(11), 3243-3258. https://doi.org/10.1061/(ASCE)0733-9445(1994)120:11(3243)

Bertola, N.J., Papadopoulou, M., Vernay, D. and Smith, I.F.C. (2017), "Optimal multi-type sensor placement for structural identification by static-load testing", *Sensors*, **17**(12). https://doi.org/10.3390/s17122904

Brownjohn, J., Fujino, Y., Inaudi, D. and Wu, Z. (2008), "Structural identification of constructed systems: experimental considerations", *Proceedings of ASCE Structures Congress 2008*, Vancouver, Canada, April, pp. 1-13. https://doi.org/10.1061/41016(314)139

Chen, X.Z., Zhu, H.P. and Chen, C.Y. (2005), "Structural damage identification using test static data based on grey system theory", *J. Zhejiang Univ. Sci.*, **6A**(8), 790-796. https://doi.org/10.1631/jzus.2005.A0790

Deep, K., Singh, K.P., Kansal, M.L. and Mohan, C. (2009), "A real coded genetic algorithm for solving integer and mixed integer optimization problems", *Appl. Math. Comput.*, **212**(2), 505-518. https://doi.org/10.1016/j.amc.2009.02.044

Emadi, S., Lozano-Galant, J.A., Xia, Y., Ramos, G. and Turmo, J. (2019), "Structural system identification including shear deformation of composite bridges from vertical deflections", *Steel Compos. Struct., Int. J.*, **32**(6), 731-741. https://doi.org/10.12989/scs.2019.32.6.731

Farrar, C.R., Baker, W.E., Bell, T.M., Cone, K.M., Darling, T.W., Duffey, T.A., Eklund, A. and Migliori, A. (1994), "Dynamic characterization and damage detection in the I-40 bridge over the Rio Grande", Research Report No. LA-12767-MS; Los Alamos National Laboratory, USA. https://doi.org/10.2172/10158042

Hajela, P. and Soeiro, F.J. (1990), "Recent developments in damage detection based on system identification methods", *Struct. Optimiz.*, **2**(1), 1-10. https://doi.org/10.1007/BF01743515

Hjelmstad, K.D. and Shin, S. (1997), "Damage detection and assessment of structures from static response", *J. Eng. Mech.*, **123**(6), 568-576. https://doi.org/10.1061/(ASCE)0733-9399(1997)123:6(568)

Kim, J.-T., Ryu, Y.-S., Cho, H.-M. and Stubbs, N. (2003), "Damage identification in beam-type structures: frequency-based method vs mode-shape-based method", *Eng. Struct.*, **25**(1), 57-67. https://doi.org/10.1016/S0141-0296(02)00118-9

Kourehli, S.S. (2017), "Plate-like structures damage detection based on static response and static strain energy using gaussian process regression (GPR)", *Inverse Probl. Sci. Eng.*, **26**(8), 1198-1213. https://doi.org/10.1080/17415977.2017.1386188

Lei, J., Nogal, M., Lozano-Galant, J.A., Xu, D. and Turmo, J. (2018), "Constrained observability method in static structural system identification", *Struct. Control Health Monitor.*, **25**(1), 2040e. https://doi.org/10.1002/stc.2040

Lei, J., Lozano-Galant, J.A., Xu, D. and Turmo, J. (2019), "Structural system identification by measurement error-minimizing observability method", *Struct. Control Health Monitor.*, **26**(10), e2425. https://doi.org/10.1002/stc.2425

Li, D.-S., Li, H.-N. and Fritzen, C.-P. (2012), "Load dependent sensor placement method: Theory and experimental validation", *Mech. Syst. Signal. Pr.*, **31**, 217-227. https://doi.org/10.1016/j.ymssp.2012.04.014

Li, S., Dong, J., Lu, W., Li, H., Xu, W. and Jin, Y. (2017), "Optimal sensor placement for cable force monitoring using spatial correlation analysis and bond energy algorithm", *Smart Struct. Syst., Int. J.*, **20**(6), 769-780. https://doi.org/10.12989/sss.2017.20.6.769

Liu, C., Teng, J. and Peng, Z. (2020), "Optimal sensor placement for bridge damage detection using deflection influence line", *Smart Struct. Syst., Int. J.*, **25**(2), 169-181. https://doi.org/10.12989/sss.2020.25.2.169

Lozano-Galant, J.A., Nogal, M., Castillo, E. and Turmo, J. (2013), "Application of observability techniques to structural system identification", *Comput.-Aided. Civil Infrastr.*, **28**(6), 434-450. https://doi.org/10.1111/mice.12004

Lozano-Galant, J.A., Nogal, M., Turmo, J. and Castillo, E. (2015), "Selection of measurement sets in static structural identification of bridges using observability trees", *Comput. Concrete, Int. J.*, **15**(5), 771-794. https://doi.org/10.12989/cac.2015.15.5.771

Ma, Q. and Solís, M. (2018), "Damage localization and quantification in beams from slope discontinuities in static deflections", *Smart Struct. Syst., Int. J.*, **22**(3), 291-302. https://doi.org/10.12989/sss.2018.22.3.291

Meo, M. and Zumpano, G. (2005), "On the optimal sensor placement techniques for a bridge structure", *Eng. Struct.*, **27**(10), 1488-1497. https://doi.org/10.1016/j.engstruct.2005.03.015

Nguyen, V.H., Schommer, S., Maas, S. and Zürbes, A. (2016), "Static load testing with temperature compensation for structural health monitoring of bridges", *Eng. Struct.*, **127**, 700-718. https://doi.org/10.1016/j.engstruct.2016.09.018

Nogal, M., Lozano-Galant, J.A., Turmo, J. and Castillo, E. (2015), "Numerical damage identification of structures by observability techniques based on static loading tests", *Struct. Infrastruct. E.*, **12**(9), 1216-1227. https://doi.org/10.1080/15732479.2015.1101143

Papadopoulos, L. and Garcia, E. (1998), "Structural damage identification - A probabilistic approach", *Astronaut. Aeronaut.*, **36**(11), 2137-2145. https://doi.org/10.2514/2.318

Peng, T., Nogal, M., Casas, J.R., Lozano-Galant, J.A. and Turmo, J. (2020), "Constrained observability techniques for structural system identification using modal analysis", *J. Sound. Vib.*, **479**, 115368. https://doi.org/10.1016/j.jsv.2020.115368

Sanayei, M. and Chitra, J. (2002), "Sensor placement for parameter estimation of structures using fisher information matrix", *Proceedings of the 7th International Conference on Applications of Advanced Technologies in Transportation*

(*AATT*), Boston Marriot, USA, August. https://doi.org/10.1061/40632(245)49

Sanayei, M., Dicarlo, C.J., Rohela, P., Miller, E.L. and Kilmer, M.E. (2015), "Sensor placement using fisher information matrix for robust finite element model updating", *Life Cycle Reliab. Saf. Eng.*, **4**(2), 28-39.

Sanayei, M. and Scampoli, S.F. (1991), "Structural element stiffness identification from static test data", *J. Eng. Mech.*, **117**(5), 1021-1036. https://doi.org/10.1061/(ASCE)0733-9399(1991)117:5(1021)

Sheena, Z., Unger, A. and Zalmanovich, A. (1982), "Theoretical stiffness matrix correction by using static test results", *Isr. J. Technol.*, **20**, 245-253.

Tan, Y. and Zhang, L. (2019), "Computational methodologies for optimal sensor placement in structural health monitoring: A review", *Struct. Health. Monitor.*, **19**(4), 1287-1308. https://doi.org/10.1177/1475921719877579

Tomàs, D., Lozano-Galant, J.A., Ramos, G. and Turmo, J. (2018), "Structural system identification of thin web bridges by observability techniques considering shear deformation", *Thin. Wall. Struct.*, **123**, 282-293. https://doi.org/10.1016/j.tws.2017.11.017

Tong, K.H., Bakhary, N., Kueh, A.B.H.H., Mohd Yassin, A.Y., Yassin, A.Y.M., Bakhary, N. and Kueh, A.B.H.H. (2014), "Optimal sensor placement for mode shapes using improved simulated annealing", *Smart Struct. Syst., Int. J.*, **13**(3), 389-406. https://doi.org/10.12989/sss.2014.13.3.389

Wang, X., Hu, N., Fukunaga, H. and Yao, Z.H. (2001), "Structural damage identification using static test data and changes in frequencies", *Eng. Struct.*, **23**(6), 610-621. https://doi.org/10.1016/S0141-0296(00)00086-9

Wang, X., Yang, H., Wang, L. and Qiu, Z. (2012), "Interval analysis method for structural damage identification based on multiple load cases", *J. Appl. Mech.*, **79**(5), 051010. https://doi.org/10.1115/1.4006447

Zhang, Y., Kim, C.W., Zhang, L., Bai, Y., Yang, H., Xu, X. and Zhang, Z. (2020), "Long term structural health monitoring for old deteriorated bridges: A Copula-ARMA approach", *Smart Struct. Syst., Int. J.*, **25**(3), 285-299. https://doi.org/10.12989/sss.2020.25.3.285

Zhou, G.D., Yi, T.H., Zhang, H. and Li, H.N. (2015), "Optimal sensor placement under uncertainties using a nondirective movement glowworm swarm optimization algorithm", *Smart Struct. Syst., Int. J.*, **16**(2), 243-262. https://doi.org/10.12989/sss.2015.16.2.243

BS